


Triple point of synchronization, phase singularity, and excitability along the transition between unbounded and bounded phase oscillations in a forced nonlinear oscillator

Willian T. Prants and Cristian Bonatto

Instituto de Física, Universidade Federal do Rio Grande do Sul, 91501-970 Porto Alegre, Brazil

 (Received 29 February 2020; revised 23 June 2020; accepted 8 February 2021; published 1 March 2021)

We report the discovery of a codimension-two phenomenon in the phase diagram of a second-order self-sustained nonlinear oscillator subject to a constant external periodic forcing, around which three regimes associated with the synchronization phenomenon exist, namely phase-locking, frequency-locking without phase-locking, and frequency-unlocking states. The triple point of synchronization arises when a saddle-node homoclinic cycle collides with the zero-amplitude state of the forced oscillator. A line on the phase diagram where limit-cycle solutions contain a phase singularity departs from the triple point, giving rise to a codimension-one transition between the regimes of frequency unlocking and frequency locking without phase locking. At the parameter values where the critical transition occurs, the forced oscillator exhibits a separatrix with a π phase jump, i.e., a particular trajectory in phase space that separates two distinct behaviors of the phase dynamics. Close to the triple point, noise induces excitable pulses where the two variants of type-I excitability, i.e., pulses with and without 2π phase slips, appear stochastically. The impacts of weak noise and some other dynamical aspects associated with the transition induced by the singular phenomenon are also discussed.

DOI: [10.1103/PhysRevE.103.032201](https://doi.org/10.1103/PhysRevE.103.032201)

I. INTRODUCTION

The synchronization phenomenon, singular phenomena, and excitability are subjects of interest in theoretical and applied sciences. Synchronization arises in several areas such as biology, chemistry, and physics [1–5]. Nonlinear oscillations play a central role in synchronization, where the case of a single macroscopic oscillator subject to a constant external periodic forcing is a relevant situation that has attracted the attention of the scientific community for a long time [6–9]. In dynamical systems, the impact of singularities, i.e., exceptional points associated with the divergence of some quantity that eventually appear in mathematical descriptions of natural phenomena, is another topic of considerable attention. For example, phase singularity is discussed by Winfree in biological contexts [1]. Other examples of singular phenomena arise in chemistry [10] and physics, including vortex dynamics [11], magnetic reconnection [12], and shock waves [13]. Last, the excitable behavior of nonlinear oscillators due to applied stimuli or random fluctuations is a relevant topic within the study of complex systems [14,15]. In particular, the excitable properties of optoelectronic devices has recently received a large amount of attention due to the possibility to mimic neuron networks to explore neurocomputational properties [16].

In this article we investigate the nonlinear dynamics of a two-dimensional self-sustained oscillator subject to a constant external periodic force, a system where the above mentioned topics are connected. Our main interest is to investigate the phase dynamics of the forced nonlinear oscillator along the transition between unbounded (drifting) and bounded (trapped) phase oscillations, where a new qualitative scenario is revealed. Unbounded and bounded phase oscillations are

generic dynamic behaviors in oscillatory systems. A simple example in physical systems comes from mechanics, where a nonlinear pendulum can exhibit a continuous turning through vertical planar circles or back and forth oscillations. As it is well known, the transition between both phase regimes, i.e., phase rotations and phase oscillations, is marked by a trajectory in phase space called separatrix [8,9,17]. Other examples of systems exhibiting transitions between phase rotations and phase oscillations arise in interacting oscillatory systems, including an electronic oscillator with injected signal [18], a pair of coupled nonlinear oscillators [19], an optically injected semiconductor laser [20], three-wave interaction [21], a dual-mode solid-state laser with self-injection [22], and a forced hydrodynamically self-excited jet [23], just to name a few. In this case, the phase difference between the forcing and perturbed oscillators can be unbounded or bounded. As it is well known, in systems able to exhibit synchronization, a phase difference constant in time corresponds to a *synchronous state*, in which both phase and frequency of the perturbed oscillator are locked to the corresponding ones of the forcing oscillation. A phase difference growing or decreasing unboundedly in time corresponds to an *asynchronous state*, in which both phase and frequency are unlocked. And a phase difference changing in time by performing bounded oscillations corresponds to a *partial synchronous state*, in which the average frequency is locked, but the phase is unlocked. This regime is usually referred to as phase trapping [18,19] or frequency locking without phase locking [22]. In recent years, there has been an increasing interest in investigations of injection-locked oscillators discriminating oscillatory regimes with unbounded and bounded phase, especially within the field of optics [24–29]. Moreover, injection-locked oscillators

constitute an important class of systems where distinct types of excitability are observed [29–45]. The fact that phase oscillations can be unbounded or bounded affects the geometrical aspects that the excitability phenomenon manifests itself, as we discuss below.

A classification of excitability was introduced by Hodgkin, in the 1940s, and it is still useful nowadays. Hodgkin identified three types (classes) of excitability, according to the type of response due to stimulus applied in squid giant axons [46]. Later, in the 1980s, Rinzel and Ermentrout explained excitability in the light of the modern dynamical bifurcation theory [47]. The various types of excitable dynamics occur because there are different transitions or bifurcations relating resting (stationary) and spiking (oscillatory) states. In Type-I excitability, excited pulses can be generated with arbitrarily low frequencies and the associated bifurcation is a saddle-node infinite period (SNIPER) bifurcation, also called saddle-node on invariant circle or saddle-node homoclinic bifurcation. In Type-II excitability, pulses are excited within a relatively narrow frequency band, and the usual associated bifurcation is the Hopf bifurcation. In Type-III excitability, the pulse repetition frequency is not defined, since there is not a sustained spiking activity. In this case, there is not a formal bifurcation associated. For further discussions about classification and geometrical aspects of excitability see, e.g., Refs. [48–51].

For small injection strengths, the transition between phase-locking and phase-unlocking regimes involves a SNIPER bifurcation, and the injection-locked oscillator exhibits Type-I excitability. By looking at the oscillator’s phase dynamics, the phase performs a 2π rotation when a pulse is excited. These are the well-known 2π phase slips that occur close to a transition from phase-locking to phase-unlocking regimes with unbounded phase, being the basic scenario of Type-I excitability observed in the Adler approximation [33,34]. For large injection strengths, the transition between phase locking and phase unlocking typically involves a Hopf bifurcation, and the injection-locked oscillator exhibits Type-II excitability [52]. In this case, the transition from phase locking to phase unlocking involves a bounded-phase limit cycle, and phase oscillations do not exhibit a full 2π rotation. This has an important physical consequence since, when crossing the Hopf bifurcation, the phase of the oscillator is unlocked from the external signal, but the average frequency remains locked, giving rise to the phase-trapping or frequency-locking without phase-locking regime [19,22].

While Type-I excitability with the phase dynamics exhibiting full 2π rotations is the most common situation appearing in the literature, dynamical scenarios involving experiments and simulations of excitable dynamics not accompanied by 2π phase rotations have been found in delay-coupled lasers [34] and in a dual-mode laser with self-injection [29]. These scenarios of bounded-phase dynamics are not due to the Type-I excitability mechanism. Only very recently, it has been found that Type-I excitable pulses can occur without being accompanied by 2π phase rotations in a dual state quantum dot laser with optical injection [45]. In this case, the excitable response depends on the interplay of two lasing states operating in antiphase. Simulations of a nine-dimensional model have identified an associated bounded-phase limit cycle when

crossing the SNIPER bifurcation, characterizing a new variant of Type-I excitability.

The aim of this manuscript is to present three main novelties. First, we show that, when the injection strength is increased in a simple planar model of an injection-locked oscillator, there is a transition from a SNIPER bifurcation with full 2π phase rotation to a SNIPER bifurcation in the bounded-phase regime. This transition corresponds to a triple point of synchronization, i.e., a codimension-two point in the phase diagram of the injection-locked oscillator where three distinct regimes of synchronization meet, namely phase-locking (PL), frequency-locking without phase-locking (FL), and frequency-unlocking (FU) states.

As we show here, a phase singularity plays an important role in this transition and we discuss in detail this point. Second, we show that, for moderate injection strengths, the limit-cycle oscillations are very sensitive to the influence of low-intensity noise. In this case, the planar injection-locked oscillator can easily exhibit noise-induced alternation between unbounded and bounded phase dynamics. Third, we show that, close to the triple point of synchronization, noise induces excitable pulses in which the two variants of Type-I excitability appear randomly. In other words, noise induces stochastic intensity pulsations that sometimes exhibit 2π phase slips and at other times do not.

The manuscript is organized as follows. We investigate theoretically a second order negative differential conductance oscillator, with cubic nonlinearity, subject to a constant external periodic forcing, whose model is presented in Sec. II. This model can describe distinct physical situations, and we address the cases of electronic and optical oscillators in Appendices A and B, respectively. In Sec. III, we investigate the deterministic aspects of the model. We present a bifurcation analysis and discuss the phase dynamics scenario, focusing on the associated dynamics due to the occurrence of a phase singularity. In Sec. IV, we investigate the influence of a low-intensity noise on the limit-cycle dynamics close to the transition between FU and FL. In Sec. V, we investigate the Type-I excitable dynamics of the injection locked oscillator. In Sec. VI, we discuss some physical considerations about the phase singularity and the impact on the dynamics of the forced oscillator caused by the collision between the limit cycle and the singular point. Finally, in Sec. VII, we present the main conclusions of this work.

II. MODEL

We investigate the dynamics of a second-order nonlinear oscillator subject to an external periodic driving, whose model is given by

$$\frac{dA}{d\tau} = (1 - |A|^2)A - j\Omega A + \kappa + D\xi(\tau), \quad (1)$$

where A represents the normalized complex amplitude of the forced oscillator, while Ω and κ represent the frequency detuning and the injection strength, respectively. The last additive term in Eq. (1) represents some generic unavoidable stochastic fluctuation affecting the oscillator’s dynamics. Here $\xi = \xi_x + i\xi_y$ is a complex noise source, where ξ_x and ξ_y are two independent white noise sources with zero mean and

unitary variance. D is the noise strength. Equation (1) can describe many distinct physical situations of a self-sustained oscillator under the influence of an external periodic signal. By writing the deterministic part of Eq. (1) in terms of amplitude and phase of the complex amplitude $A = ae^{j\phi}$, we have the following pair of equations:

$$\frac{da}{d\tau} = (1 - a^2)a + \kappa \cos \phi, \quad (2)$$

$$\frac{d\phi}{d\tau} = -\Omega - \frac{\kappa}{a} \sin \phi, \quad (3)$$

where a is the normalized amplitude of the forced oscillator, while ϕ is the phase difference between the self-sustained oscillator and the external signal. When the strength of the external signal is weak, the amplitude of the forced oscillator remains almost unchanged and Eq. (1) can be reduced to the well-known Adler equation [53] [which is Eq. (3) with $a = 1$]. Thus, Eq. (1) represents a model of a periodically driven self-sustained oscillator when amplitude perturbations just beyond the Adler approximation are taken into account. Physical situations modeled by Eq. (1) arise in, e.g., negative differential conductance devices subject to an external periodic force, such as externally driven electronic or optical oscillators. In the context of electronic oscillators, Eq. (1) is the variational equation of the forced Van der Pol oscillator [18,54,55]. It can also be obtained by modeling a nonlinear electronic circuit with an injected signal, as we illustrate in Appendix A. In the context of optics, Eq. (1) can be obtained by performing a variable transformation in the cubic laser model with optical injection, as we show in Appendix B. Equation (1) can also be obtained as a particular case of the more general problem of considering small periodic perturbations on systems exhibiting a Hopf bifurcation [56]. In this context, generalizations of Eq. (1) have been investigated in the literature, such as studies of subharmonic resonance [57] and analysis including the variation of a third parameter that controls the distance from the Hopf bifurcation [58]. In another general context, an amplitude and phase model similar to Eqs. (2) and (3) have been obtained and analyzed by Childs and Strogatz [59] by doing a reduction of the forced Kuramoto model to a low-dimensional (planar) system.

III. TRIPLE POINT OF SYNCHRONIZATION AND SEPARATRIX WITH π PHASE JUMP

Despite being two dimensional, the noise-free nonlinear oscillator described by Eq. (1) presents a relatively rich dynamical scenario due to nonlinear effects of amplitude perturbations. Many aspects of its nonlinear dynamics on variation of the injection parameters have been extensively investigated in the past and are well known [18,54–56]. Basic scenarios of transition between phase-locking states (stationary states) and phase-unlocking states (limit cycles) can be observed through saddle-node or Hopf codimension-one bifurcations, which are connected through codimension-two Bogdanov-Takens (BT) bifurcations [55]. Also, homoclinic [55] and frequency pulling [56] phenomena are well known to occur. For small injection strengths, the transition from phase-locking to phase-unlocking regimes is through a SNIPER bifurcation. As the injection strength increases, the saddle-

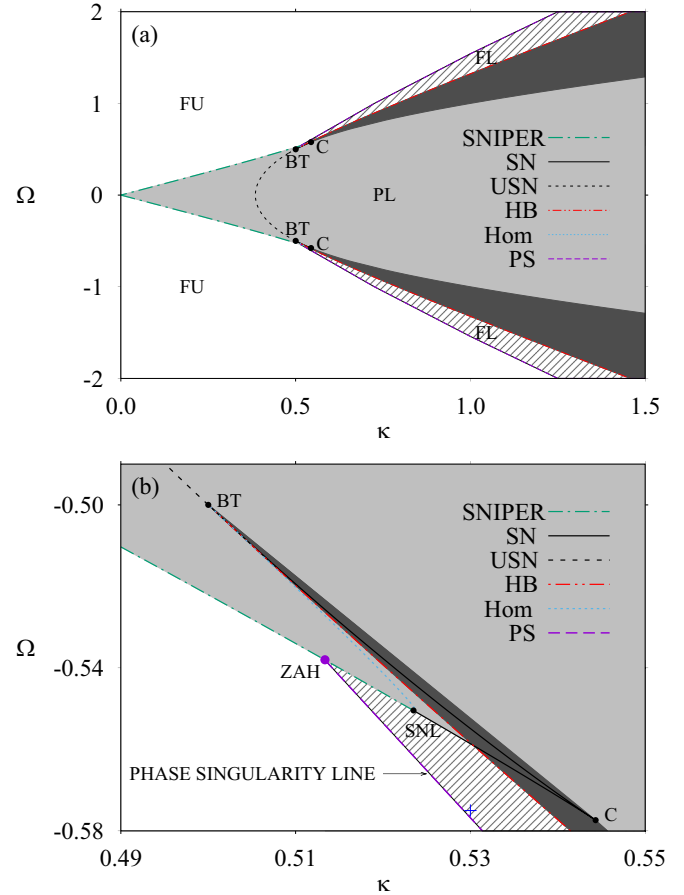


FIG. 1. Phase diagram and the associated bifurcation set of the forced nonlinear oscillator as a function of the injection parameters (κ, Ω) . A global view is shown in (a) and a magnification of the region with complex dynamics is shown in (b). Gray tones correspond to parameter regions with stable phase-locked states (PL) (light and dark gray tones denote regions with overdamped and damped relaxation oscillations, respectively). Distinct line types denote SNIPER, saddle-node (SN), unstable saddle-node (USN), Hopf (HB), and Homoclinic (Hom) bifurcations. ZAH denotes the triple point of synchronization, from which the phase singularity (PS) line emerges. BT, C, and SNL denote Bogdanov-Takens, cusp, and saddle-node loop codimension-two points, respectively. White and hatched areas correspond to frequency-unlocking (FU) and frequency-locking without phase-locking (FL) states, respectively. The dynamics related to the point marked by (+) is investigated in Sec. IV.

node limit cycle becomes noncentral at the saddle node loop codimension-two point (SNL), and a saddle homoclinic bifurcation takes place, existing up to the BT bifurcation. For large injection strengths, the transition between phase locking and phase unlocking is through a Hopf bifurcation. All this well-known scenario is illustrated in Figs. 1(a) and 1(b). Figure 1 discriminates three distinct regimes related to the synchronization properties of the forced oscillator, namely PL, FL, and FU, denoted by gray tones, hatched, and white areas, respectively. As can be seen in Fig. 1(a), the FL regime, i.e., the bounded-phase oscillatory regime, appears as an intermediate step along the complete transition between PL and FU states on crossing the Hopf bifurcation. However, the FL

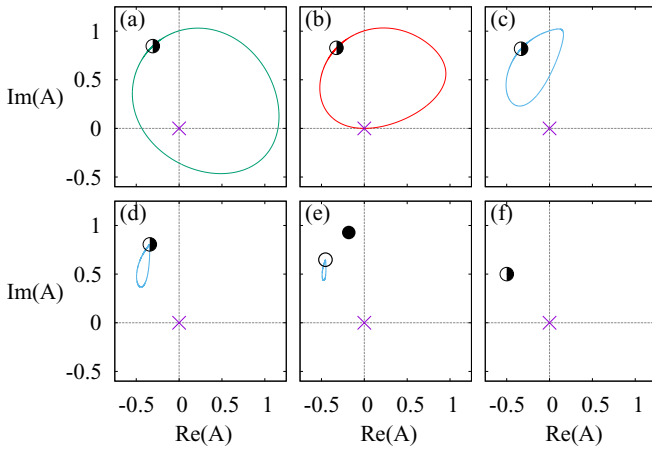


FIG. 2. Phase-space plots illustrating the evolution of the homoclinic cycles up to the BT point. (×) denotes the zero-amplitude state, (●) the saddle-node equilibrium, (○) the saddle equilibrium, and (●) the node equilibrium. The injection parameters (κ, Ω) , as well as the corresponding points marked in Fig. 1, are (a) $(0.5000, -0.5220)$ (point a), (b) $(0.5131, -0.537733)$ (ZAH point), (c) $(0.5185, -0.5443)$ (point c), (d) $(0.5235, -0.5505)$ (SNL point), (e) $(0.5185, -0.5380)$ (point e), and (f) $(0.5000, -0.5000)$ (BT point).

regime is not only associated with the Hopf bifurcation, but can also be associated with the SNIPER bifurcation, as we elucidate here [see Fig. 1(b)]. We discuss this point in detail below.

A situation that has not been fully investigated until now is related to the transition between FU and FL states. This codimension-one transition between unbounded and bounded phase oscillations in an injection-locked oscillator were studied by Cartwright a long time ago [18]. Here we show that this transition originates at a special codimension-two point located at the SNIPER bifurcation, denoted by ZAH in Fig. 1(b). At this point, the zero-amplitude state of the forced oscillator collides with the SNIPER orbit, i.e., a homoclinic orbit containing a saddle-node equilibrium point. The ZAH point corresponds to a triple point of synchronization, where the three regimes FU, FL, and PL meet. To better understand the scenario of the phase dynamics along the SNIPER bifurcation, we plot the homoclinic orbits for some representative injection parameter values in Fig. 2. The homoclinic orbits were obtained with AUTO [60] by numerical integration of Eq. (1) without the noise term and depicted as functions of the components of the complex amplitude $A = a_x + ia_y$. A SNIPER orbit associated with the appearance or disappearance of limit cycles with unbounded phase, which occurs for small injection strengths, is illustrated in Fig. 2(a). It is easy to see that, since the origin $(\text{Re}(A), \text{Im}(A)) = (0, 0)$ is in the interior of the orbit connecting the saddle-node equilibrium, the phase performs a full 2π rotation around the origin. As the injection strength increases, a critical transition takes place at the ZAH point, where the SNIPER bifurcation starts to be associated with bounded-phase limit cycles, as shown in Fig. 2(b). At this critical point, located at $(\kappa, \Omega) \approx (0.5131, -0.537733)$, the homoclinic orbit connects the zero-amplitude state of the oscillator to the saddle-node equilibrium. The zero-amplitude

state is a point of phase singularity in time, where the amplitude of the oscillator is zero, and the phase is indeterminate. For injection strengths above the ZAH point, the origin does not lie in the interior of the saddle-node homoclinic cycle, and the phase will not perform a full 2π rotation anymore, remaining bounded with rotation angles less than π . A bounded-phase SNIPER orbit is shown in Fig. 2(c) and exists up to the SNL point, determined with AUTO to be located at $(\kappa, \Omega) \approx (0.5235, -0.5505)$ [Fig. 2(d)]. After this point, the scenario is well known: There is a separation in parameter space between the saddle homoclinic orbit and the saddle-node equilibrium, originating multistability, as illustrated in Fig. 2(e). The saddle homoclinic bifurcation advances inside the locking region until it disappears at the BT point illustrated in Fig. 2(f).

The transition between unbounded and bounded phase oscillations can also be analyzed by writing Eq. (1) in terms of phase and amplitude. In Fig. 3(a), we show some representative SNIPER orbits (denoted by the dashed blue lines) for parameter values in between the ZAH and SNL points. The critical SNIPER orbit at the ZAH point, connecting the zero-amplitude state to the saddle-node equilibrium (shown by the dot), is plotted in solid red line. As can be seen, when the amplitude is zero, a phase singularity occurs and there is a jump of π rad in the phase of the oscillator. A line of phase singularity in the parameter space, where limit-cycle solutions contain the zero amplitude state, departs from the ZAH point, giving rise to the codimension-one transition between FU and FL states, what Cartwright denominated “critical drift” [18]. This transition does not correspond to a bifurcation when the equations are written in Cartesian coordinates, but it does correspond to a bifurcation when they are expressed in polar coordinates, as discussed in the literature [20]. In Fig. 1(b), the phase singularity line is denoted by the dashed purple line, separating the white area (FU states) and the hatched area (FL states). In Fig. 3(b), we illustrate some orbits with bounded phase oscillations (denoted by the dashed blue lines) and an orbit at the critical transition, i.e., over the phase singularity line (denoted by the solid red line). As can be seen, the limit cycle containing the phase singularity exhibits a jump of π in its phase. In this case, the period of the limit cycle is finite, in contrast to the case over the SNIPER bifurcation, where the period of the cycle is infinite due to the presence of the saddle-node equilibrium connected to the orbit. The jump of π in the oscillator’s phase occurs instantaneously, i.e., with an infinite speed. Equation (3) already suggests the divergence of the phase speed when the amplitude of the injection-locked oscillator vanishes. In Fig. 3(c), we plot the phase velocity of the oscillator as a function of the phase for some bounded-phase orbits. The phase speed increases when approaching the phase singularity line, as shown in Fig. 3(d). A time series in the unbounded phase regime, very close to the phase singularity line, is shown in Fig. 3(e), where the curve almost touches the zero-amplitude state. The corresponding phase dynamics is shown in Fig. 3(f), where the phase of the oscillator exhibits a π jump.

The dynamics along the transition between the FU and FL states is further illustrated in Fig. 4. The left and right columns depict the oscillator’s dynamics in the FU and FL regimes, respectively. As can be seen in Figs. 4(a)–4(d), the oscillator’s

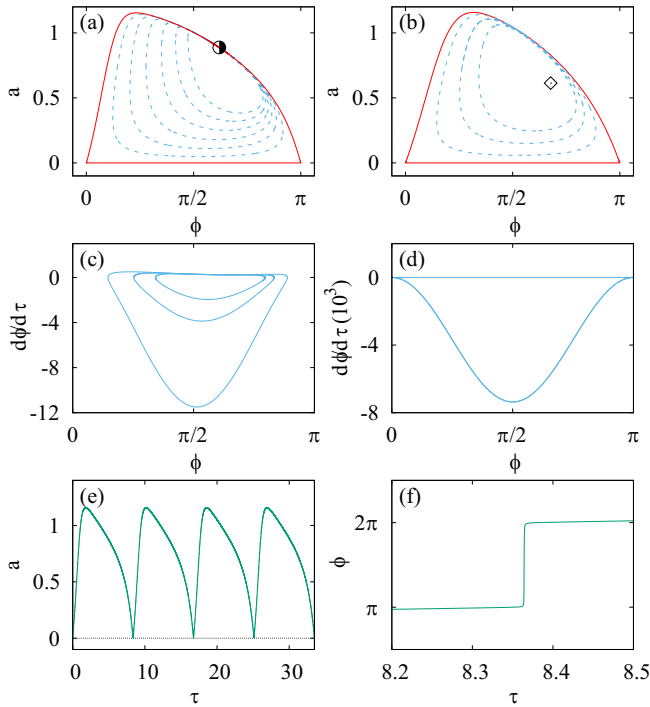


FIG. 3. (a) Amplitude as a function of phase for distinct injection parameter values over the SNIPER bifurcation. The parameter values corresponding (from the smallest to the largest) to the limit cycles denoted by the dashed blue lines are $(\kappa, \Omega) = (0.519, -0.545), (0.518, -0.544), (0.517, -0.542), (0.516, -0.541), (0.515, -0.540),$ and $(0.514, -0.539)$. The orbit denoted by the solid red line and the saddle-node equilibrium (\blacklozenge) correspond to the ZAH point located approximately at $(0.5131, -0.5377)$. (b) Illustration of bounded-phase orbits for $(\kappa, \Omega) = (0.75, -1), (0.74, -1)$ and $(0.73, -1)$, corresponding (from the smallest to the largest) to the limit cycles denoted by the dashed blue lines. The solid red line is the critical orbit containing the phase singularity located approximately at $(0.723118, -1)$, and (\diamond) marks the unstable focus equilibrium. (c) Phase speed versus phase corresponding to the three orbits denoted by the dashed blue lines in (b). (d) Phase speed versus phase for $(\kappa, \Omega) = (0.72313, -1)$, close to the phase singularity line. (e) Amplitude as a function of time and (f) phase as a function of time for $(\kappa, \Omega) = (0.72311, -1)$, very close to the phase singularity line. Angles are in radians.

phase is unbounded in the FU regime and bounded (less than π) in the FL regime. Since the injection parameters are close to the phase singularity line, the phase speed exhibits large values when the oscillator approaches the zero-amplitude state, as shown in Figs. 4(e) and 4(f). It can also be seen that $d\phi/d\tau$ is strictly positive in the FU regime [Fig. 4(e)] and changes sign in the FL regime [Fig. 4(f)].

The critical limit cycles containing the phase singularity appear as a separatrix in phase space. In Fig. 5, we present some distinct behaviors of the phase dynamics on varying the initial conditions. The injection parameters are chosen very close to the phase singularity line, according to some numerical precision. When the initial conditions lie in the interior of the limit cycle, the orbit remains bounded (shown by the solid light blue line). When the initial conditions lie outside the limit cycle, the orbit performs one or more rotations by an

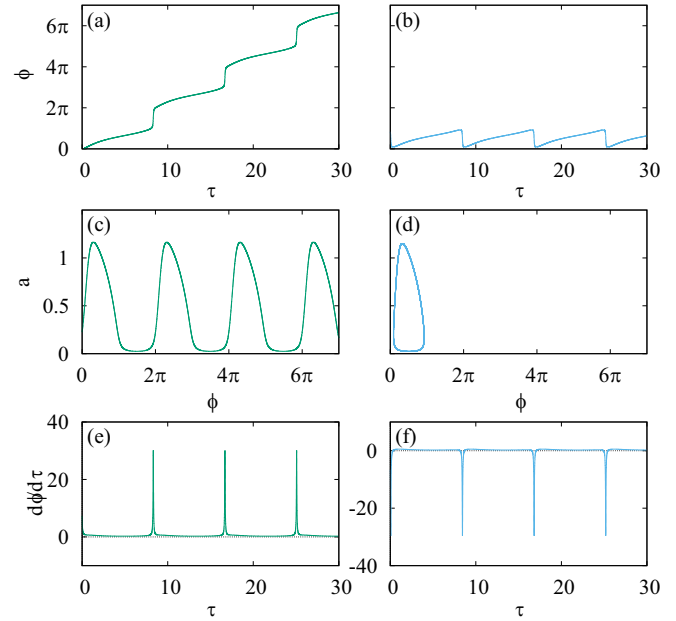


FIG. 4. Contrast between frequency-unlocking states (left column) and frequency-locking without phase-locking states (right column). The injection parameters are in the vicinity of the phase singularity line that marks the transition between these two regimes. The parameter values are $(\kappa, \Omega) = (0.72, -1)$, for the left column, and $(0.726, -1)$, for the right column. Angles are in radians.

angle greater than 2π , until being trapped in a bounded phase oscillation for larger values of the phase (shown by dotted dark blue and dashed yellow lines). The critical limit cycles containing the phase singularity [such as that illustrated by the solid red line in Fig. 3(b)] are closely related to the so-called limit phase trajectories investigated in several oscillatory sys-

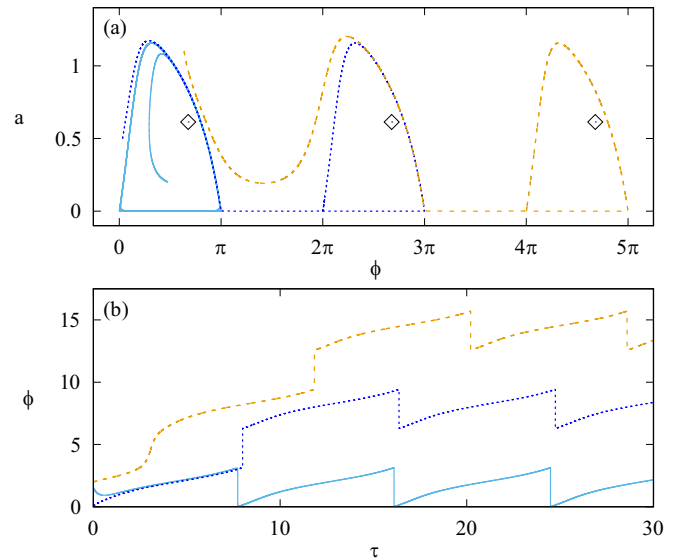


FIG. 5. (a) Amplitude versus phase and (b) phase versus time for three distinct initial conditions. (\diamond) marks the unstable focus equilibria. Injection parameters $(\kappa, \Omega) = (0.72312, -1)$ are set approximately at the critical transition (phase singularity line). Angles are in radians.

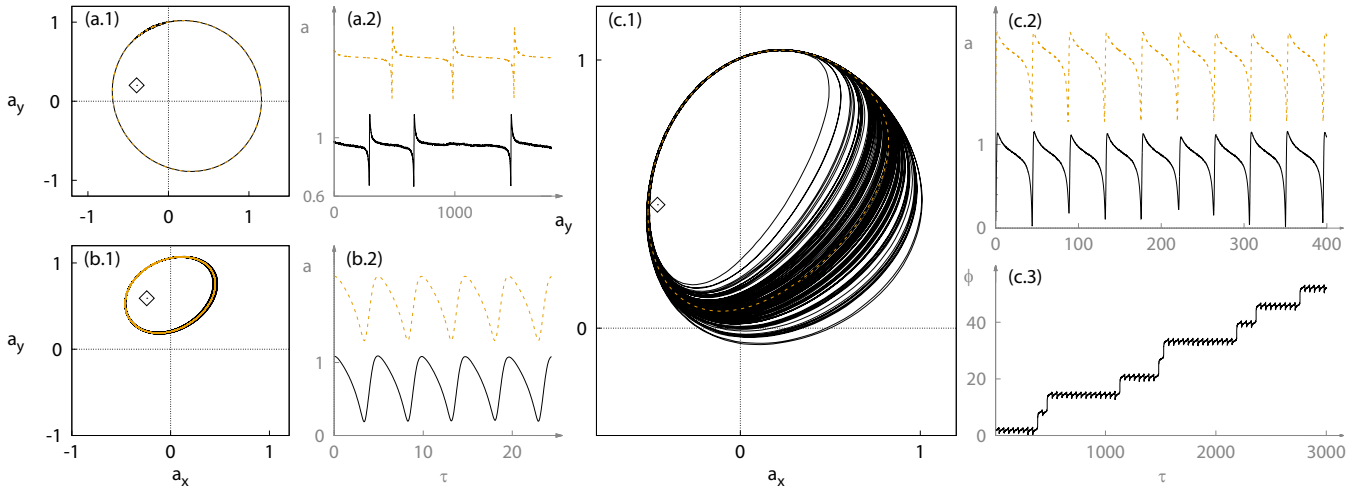


FIG. 7. Noisy (solid black lines) and deterministic (dashed yellow lines) dynamics for (a) weak, (b) strong, and (c) moderate injection strengths. The injection parameters (κ, Ω) are (a) $(0.4, -0.4098)$, (b) $(1.0, -1.45)$, and (c) $(0.53, -0.575)$. The latter point is indicated by (+) in Fig. 1(b). (\diamond) marks the unstable focus equilibrium. Angles are in radians.

and the amplitude waveform almost does not change in the presence of weak noise. A similar picture is observed for large injection strengths, when the locking-unlocking transition is dominated by the Hopf bifurcation scenario, and the forced oscillator exhibits bounded-phase limit cycles when becoming unlocked. Also in this case, weak noise has little impact over the limit-cycle dynamics, and amplitude fluctuations are not so significant, as depicted in Figs. 7(b.1) and 7(b.2). On the other hand, for the case of moderate injection strengths, the forced oscillator operates close to the transition between the SNIPER and Hopf bifurcation scenarios. In this case, the limit-cycle solutions are very sensitive to stochastic fluctuations, even weak noise, as illustrated in Fig. 7(c). The impact of weak noise for a moderate injection strength can be seen in Fig. 7(c.1), where large fluctuations in the limit-cycle dynamics occur due to the weak noise influence, in contrast with the deterministic case. Moreover, an alternation between unbounded- and bounded-phase limit cycles can be easily observed even if the injection parameters are set not so close to the phase singularity line, as is the case of Fig. 6. It is very interesting to observe that the largest noisy limit-cycle oscillation, shown in Fig. 7(c.1), resembles the limit cycle provenient from the SNIPER bifurcation, shown in Fig. 7(a.1), while the smallest noisy limit-cycle oscillation, shown in Fig. 7(c.1), resembles the limit cycle provenient from the Hopf bifurcation, shown in Fig. 7(b.1). Clearly, for moderate injection strengths, there is a mix between the SNIPER and Hopf bifurcation scenarios, making the phase space of the forced oscillator much more sensitive to stochastic fluctuations. In this case, the amplitude fluctuations due to the influence of weak noise are of much larger magnitude than those shown in Fig. 6, and they can be easily observed without the logarithmic scale, as shown in Fig. 7(c.2). In Fig. 7(c.3), we present the phase dynamics exhibiting a stochastic alternation between the unbounded- and bounded-phase limit cycles induced by the weak noise, after properly converting the Cartesian coordinates integrated from Eq. (1) to polar coordinates with continuous phase evolution.

V. STOCHASTIC INTERPLAY BETWEEN VARIANTS OF TYPE-I EXCITABILITY

In this section, we investigate the Type-I excitable dynamics of the forced nonlinear oscillator described by Eq. (1). Since we consider the complex stochastic term $D\xi(\tau)$ by integrating Eq. (1) in Cartesian coordinates, both amplitude and phase of the forced oscillator are affected by the noise influence. All the results of this section could also be obtained by directly integrating Eqs. (2) and (3) by adding the appropriate transformation of the complex noise term, or even in the simpler situation where amplitude perturbations are neglected and the noise is applied only in the phase equation.

A magnification of the injection parameter space close to the transition point (ZAH point) over the SNIPER bifurcation, which marks the change from full 2π rotations to bounded phase rotations, is shown in Fig. 8. When the bounded phase limit cycle is born through the homoclinic bifurcation (the

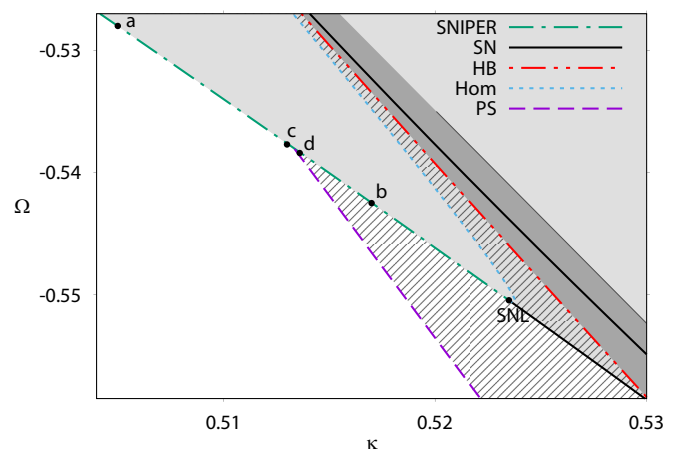


FIG. 8. Magnification of the vicinity of the triple point of synchronization ZAH shown in Fig. 4. The excitable dynamics of the points labeled a–d is shown in Fig. 9.

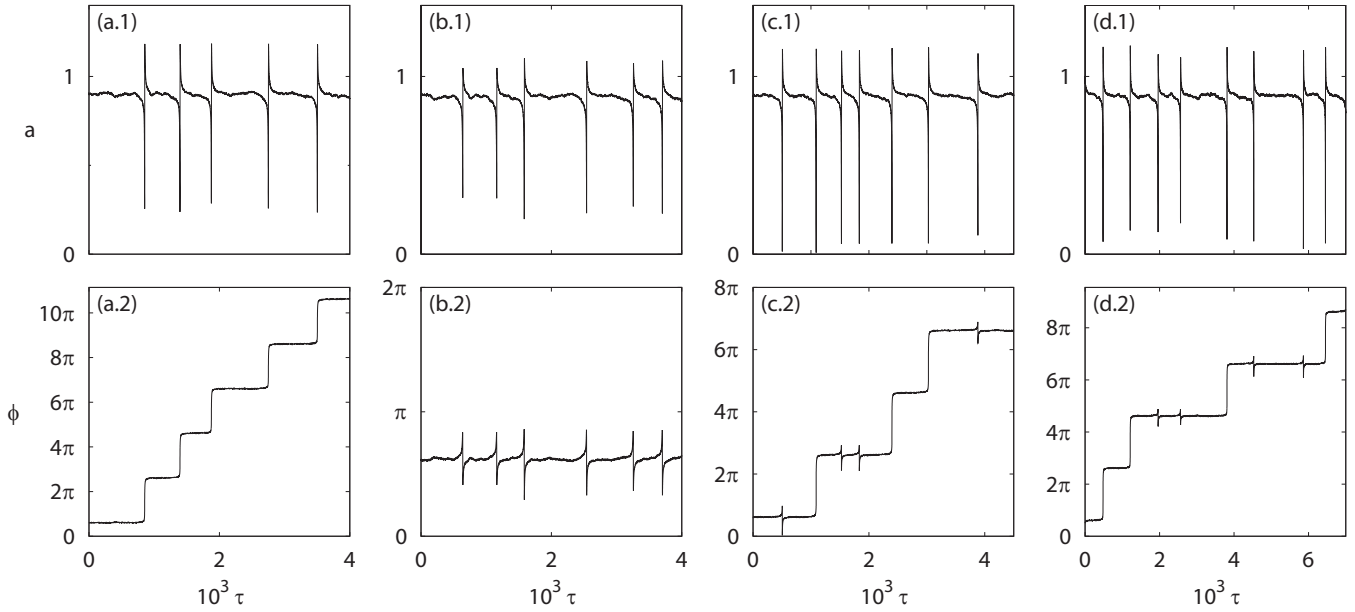


FIG. 9. Distinct qualitative scenarios of Type-I excitability. (a) Excitable pulses with 2π phase slips for $\kappa = 0.5050$ and $\Omega = -0.5280$. (b) Excitable pulses without 2π phase slips for $\kappa = 0.5170$ and $\Omega = -0.5425$. (c) Stochastic behavior of pulses with and without 2π phase slips close to the transition point ZAH for $\kappa = 0.5130$ and $\Omega = -0.5377$. (d) The same as (c), but beyond the transition point ZAH for $\kappa = 0.5136$ and $\Omega = -0.5384$. The noise amplitude is fixed at $D = 0.002$.

blue line in Fig. 8), the forced oscillator exhibits bistability. When the bounded phase limit cycle is born through the SNIPER bifurcation (the green line in Fig. 8), the forced oscillator exhibits Type-I excitability.

When looking at the oscillator's phase dynamics, the forced oscillator can exhibit three distinct qualitative scenarios for the noise-induced Type-I excitable pulses, as illustrated in Fig. 9. For small injection strengths, when the SNIPER bifurcation is associated with unbounded-phase limit cycles, the excitable pulses exhibit only 2π phase rotations [Fig. 9(a)]. This is the typical qualitative scenario observed in the Adler approximation. For large-enough injection strengths, when the SNIPER bifurcation is associated with bounded phase limit cycles, the excitable pulses never exhibit 2π phase rotations [Fig. 9(b)]. This characterizes a new variant of Type-I excitability. As we have mentioned in the introduction of the manuscript, Type-I excitable pulses in the bounded-phase regime have already been observed in Ref. [45]. But there the physical situation is more complex, involving a nine-dimensional system, where the return to the steady state involves relaxation oscillations. Here the new variant of Type-I excitable dynamics appears in a two-dimensional oscillator, due to amplitude perturbations just beyond the Adler approximation. Moreover, the new variant of Type-I excitability observed here does not exhibit relaxation oscillations. As can be seen in Fig. 8, the Hopf bifurcation and the associated saddle focus equilibrium solutions (the dark gray region), where the forced oscillator exhibits relaxation oscillations, are considerably distant from the SNIPER bifurcation.

A new qualitative scenario for the phase dynamics is shown in Figs. 9(c) and 9(d). When the injection parameters are close to the ZAH point at the SNIPER bifurcation, noise induces excitable pulses that sometimes exhibit 2π phase slips and at other times do not [Fig. 9(c)]. The alternation between phase

dynamics with or without 2π phase slips occurs in a very random way, characterizing a stochastic behavior between the two variants of Type-I excitability. It is important to mention that this behavior is not exclusive for the transition point. Even if the phase-locked oscillator operates beyond the transition point, i.e., where the SNIPER bifurcation is associated with bounded phase limit cycles, noise can still excite pulses with 2π phase slips [Fig. 9(d)]. Thus, there is a range of parameters in the vicinity of the SNIPER bifurcation where noise can excite both variants of Type-I excitability. This range depends, of course, on the noise's amplitude. By considering the same level of noise used in Figs. 9(a)–9(c) for the injection parameters denoted by the point d in Fig. 8, 2π phase jumps are not observed. However, increasing the level of noise, the stochastic behavior between the two variants of Type-I excitability is observed, as shown in Fig. 9(d).

VI. PHYSICAL CONSIDERATIONS ABOUT THE PHASE SINGULARITY AND ITS IMPACT

In this section we draw some physical considerations about the phase singularity and its connection with the transition between unbounded- and bounded-phase regimes. As already mentioned, by writing Eq. (1) in polar coordinates, there is a qualitative change of the phase dynamics on the switching between FU and FL regimes, which can be easily identified by looking at the phase-space trajectories. However, by writing Eq. (1) in Cartesian coordinates, there is no qualitative change in the limit-cycle trajectory on crossing this transition [see Figs. 10(a)–10(c)]. Therefore, it is instructive to understand better what is happening with the limit-cycle dynamics and what are some physical quantities associated with this transition.

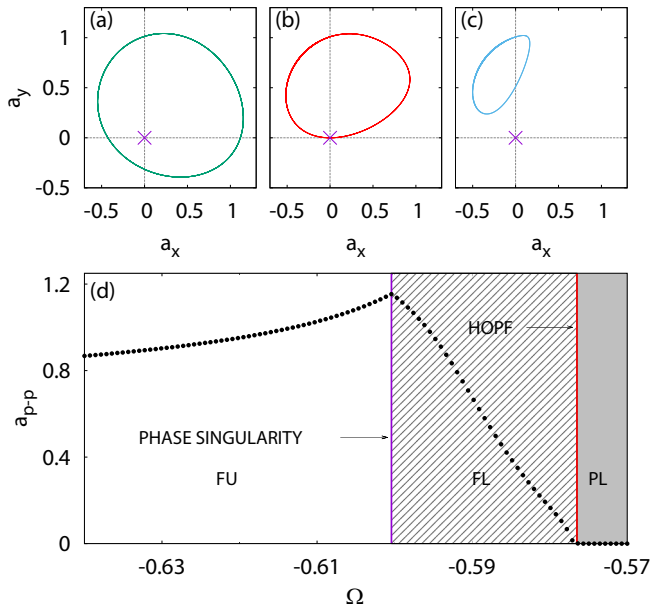


FIG. 10. Limit cycles in Cartesian coordinates for (a) $\Omega = -0.63$ (FU), (b) $\Omega = -0.60035$ (transition point), and (c) $\Omega = -0.59$ (FL). (d) Peak to peak amplitude (a_{p-p}) as a function of Ω . The injection strength is fixed at $\kappa = 0.54$.

Before providing some general considerations about the questions above, we first discuss a realistic physical situation modeled by Eq. (1), in order to understand better some physical aspects associated with the singular phenomenon. Let us consider a simple deterministic laser system (which is described in Appendix B). Without gain (pump) and external force, the laser is in the off state, i.e., there is no light inside the optical cavity. When the gain overcomes the losses (i.e., the laser operates above threshold), the laser starts to emit light with constant frequency and constant amplitude (note that, in the simple laser model described by Eq. (1), the fast optical frequency has been averaged). By writing the laser equations in terms of the electric field components, the transition from the laser-off state ($|E| = 0$) to the laser-on state ($|E| = \text{const}$) is given by a Hopf bifurcation (by writing the laser equations in terms of amplitude or intensity, the transition is given by a pitchfork or transcritical bifurcation, respectively). By considering that the gain is small enough, we have the classical case of a self-sustained oscillator close to a Hopf bifurcation. When an external force is added to the laser, e.g., by injecting light from another laser with some similar frequency, the free-running laser dynamics changes. If the external force is weak, then this change will be small, and the laser amplitude will be a bit greater or less than the free-running laser amplitude. But if the external force is strong enough, then the laser amplitude can eventually vanish. This means that the laser-on state can instantaneously interact with the laser-off state during the laser oscillations. The laser-on and laser-off states are qualitatively distinct physical states. For example, in the laser-on state, it is possible to decrease the amplitude (intensity) due to the interaction with the external force (by some sort of interference phenomenon). But in the laser-off state, it is not possible to do that, since $|E| = 0$ is already the minimum amplitude state, and it cannot be

negative. Indeed, the laser-off state is a very particular physical state of the laser system. In the presence of the external force, the laser-off state is not an equilibrium state (neither stable nor unstable), but it is a singular point, i.e., a zero-amplitude (or phaseless) state. This singular point marks a limit (or a border) in the phase space where the trajectory can evolve in a certain regime. When the trajectory touches the singular point, occurs a change in the dynamics of the system, corresponding to a physical transition in the system.

We now turn back to the limit-cycle evolution of Eq. (1) in the Cartesian plane. In Fig. 10, we show the evolution of the limit cycle when the frequency detuning is varied, for a fixed injection strength. When the frequency detuning is large, the interaction between the external force and the oscillator is not so strong, and the resulting dynamical scenario is similar to the free-running oscillator but with a varying amplitude [Fig. 10(a)]. In this case, the phase and frequency of the oscillator are unlocked, and the magnitude of the phase difference grows unboundedly. By decreasing the frequency detuning, the interaction between the external force and the oscillator gets stronger and, eventually, the limit-cycle dynamics touches the singular point (zero-amplitude state) [Fig. 10(b)]. By keeping the decrease in the frequency detuning, the interaction between the external force and the oscillator increases even more, which leads to a switching to the FL regime [Fig. 10(c)]. In this case, the oscillator and the external force oscillate with the same average frequency, meaning that the oscillator is “captured” by the external force. While in the Cartesian plane we do not see any significant change in the limit-cycle dynamics by crossing this transition, the dynamics of the oscillator is different in each side. This is illustrated in Fig. 10(d), where we plot the peak-to-peak amplitude a_{p-p} , i.e., the difference between peak and trough of the amplitude oscillations, as a function of frequency detuning. As can be seen, a_{p-p} reaches its maximum value precisely when the limit cycle touches the phase singularity (the zero-amplitude state). This means that the limit cycle containing the phase singularity (which is the separatrix trajectory in polar coordinates) maximizes the variation between the minimum and the maximum of the amplitude oscillations. In the example mentioned above, in the context of the laser dynamics, we should observe the largest variation from dark to bright light emission at the critical transition caused by the phase singularity. Moreover, in Fig. 10, we can observe that a_{p-p} follows very different functional forms in each side of the transition between the FU and FL regimes. Therefore, if we had access only to the amplitude (or intensity) time series as a function of frequency detuning, then we could identify the FU-FL transition without any information of the phase dynamics.

It is worth noting that the concepts of unbounded and bounded phase are well defined when taking the origin of the reference frame as being the equilibrium state of the unforced system. In this way, when an external force acts on the system, a restoring force appears associated with the displacement with respect to the equilibrium state. The magnitude of this displacement is a physically relevant amplitude. In the presence of a constant external force of not so large magnitude (for example, a constant pump in the context of the simple laser model discussed above), the equilibrium state, which is

the zero-amplitude state, moves to a new steady state with nonzero amplitude. In this situation, the phase singularity is a physically relevant state of the system. By changing the reference frame, e.g., by translating the origin, the new amplitude and phase variables may lose their physical meaning. In this case, the concepts of unbounded and bounded phase, as well as the phase singularity, will be relative to the choice of the origin of the reference frame. But, in this situation, the equilibrium state of the unforced system will be translated to nonzero coordinates while still being a physically relevant singular point. Therefore, even in a new reference frame, when a limit cycle of the forced system collides with the singular point, there will be a physically relevant transition. In this case, the peak to peak amplitude with respect to the singular point will be maximized at the critical transition, and the scenario described in Fig. 10 will hold, irrespective of the choice of the origin of the coordinate system.

As we discuss above, the singular point is physically relevant, and the collision between the singular point and the limit-cycle dynamics marks the change between two distinct physical states. In Cartesian coordinates, there is not a formal bifurcation associated with this transition, since there is not a topological change in the limit-cycle dynamics itself. However, the relevant aspect in this transition is the location of the singular point in relation to the limit-cycle trajectory in phase space. When the singular point lies in the interior of the limit cycle, it represents one qualitative scenario, corresponding to one physical regime. When the singular point lies in the exterior of the limit cycle, it represents another qualitative scenario, corresponding to another physical regime. And when the singular point is located on the limit cycle, it corresponds to the transition point, i.e., the critical point of the qualitative change induced by the singularity.

VII. CONCLUSION

We have reported the discovery of a triple point of synchronization in the phase diagram of a simple two-dimensional forced nonlinear oscillator, around which three regimes associated with the synchronization phenomenon exist, namely phase-locking, frequency-locking without phase-locking, and frequency-unlocking states. By increasing the injection strength of the planar injection-locked oscillator, there is a qualitative change in the phase dynamics of the SNIPER bifurcation, in which the associated homoclinic cycles change from full 2π phase rotations to bounded-phase rotations (less than π). This means that, when amplitude perturbations are taken into account in an injection-locked oscillator just beyond the Adler approximation, the SNIPER bifurcation is associated with the transition between phase-locking and frequency-unlocking states for small injection strengths, and between phase-locking and frequency-locking without phase-locking states for large injection strengths.

The triple point of synchronization, i.e., the transition point on the SNIPER bifurcation that marks the change between the two phase regimes, occurs when the homoclinic cycle with the saddle-node equilibrium is connected to a phase singularity point, i.e., an instantaneous zero-amplitude state of the forced oscillator. A line in parameter space where limit cycles contain a phase singularity departs from the triple point, giving

rise to the codimension-one transition between frequency-unlocking and frequency-locking without phase-locking states.

Trajectories containing a phase singularity appear as a separatrix in phase space, where the oscillator exhibits a π phase jump. In the classical case of separatrix observed, e.g., in the nonlinear pendulum dynamics, the phase-space trajectories connect equilibrium states, and the phase speed vanishes at the critical point. In the case investigated here, the separatrix trajectory is connected to the zero-amplitude state of the oscillator, and the phase speed diverges at the critical point.

We have investigated the impacts of stochastic fluctuations close to the phase singularity line. We have shown that, for large injection strengths, weak noise can induce an alternance between unbounded and bounded phase dynamics very close to the phase singularity line. However, for moderate injection strengths, the limit-cycle solutions are much more sensitive to the presence of noise. In this case, the deterministic limit cycles are highly disturbed, exhibiting a range from small to large excursions in the phase plane due to the presence of weak noise. Thus, the noise-induced alternance between unbounded and bounded phase dynamics can occur even if the injection parameters are set not so close to the vicinity of the phase singularity line.

We have investigated the excitable dynamics of the planar injection-locked oscillator. We have shown that this simple two-dimensional system can exhibit two variants of Type-I excitability, i.e., excitable pulses with and without 2π phase slips. The new variant of Type-I excitability, i.e., the dynamics of excitable pulses without 2π phase slips, occurs due to amplitude perturbations just beyond the Adler approximation. In this simple situation, the Type-I excitable pulses do not exhibit relaxation oscillations when returning to the phase-locked state. We have also shown that, when the injection-locked oscillator is operating phase-locked close to the triple point of synchronization, noise can induce excitable pulses that appear with or without 2π phase slips in a random way. Thus, both variants of Type-I excitability can appear stochastically due to random fluctuations.

We have discussed the physical relevance of the transition induced by the singular point. When the limit-cycle oscillations collide with the singular point, the peak-to-peak amplitude reaches its maximum value (for a fixed injection strength), i.e., the highest gradient of the amplitude variations is observed. This means that the transition between frequency locking without phase locking and frequency unlocking could be identified by measuring only the time series of the amplitude (or intensity) oscillations, i.e., without any information about the phase dynamics. We have also shown that the variation of the peak-to-peak amplitude as a function of frequency detuning follows very different functional forms in each side of the transition between frequency unlocking and frequency locking without phase locking.

Here applications of the amplitude and phase planar model have been illustrated in a forced electronic circuit and in a cubic laser with optical injection, which is an approximation of a class-A laser with optical injection. However, the model is very general and should be applicable to a variety of other systems when amplitude perturbations are taken into account just beyond the Adler approximation. Moreover, the phenomena

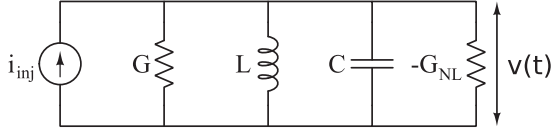


FIG. 11. Equivalent circuit diagram of a negative differential conductance oscillator with injection signal $i_{inj}(t)$.

investigated here should also appear in more complex models, either planar or with higher dimensionality. We believe that our main findings can be experimentally verified in the near future.

ACKNOWLEDGMENTS

This study was financed in part by Coordenação de Aperfeiçoamento de Pessoal de Nível Superior, Brazil (CAPES), Finance Code 001. W.T.P. thanks Conselho Nacional de Desenvolvimento Científico e Tecnológico (CNPq), Brazil, for support. The authors thank Júlio R. Schoffen for very helpful suggestions.

APPENDIX A: NEGATIVE DIFFERENTIAL CONDUCTANCE ELECTRONIC OSCILLATOR WITH INJECTION SIGNAL

A generic LC oscillator, where $1/G$ represents the losses of the oscillator, in parallel to a nonlinear element G_{NL} is shown in Fig. 11. The oscillator is driven by an external periodic signal

$$i_{inj}(t) = GV_{inj}\exp(j\omega_{inj}t), \quad (\text{A1})$$

where V_{inj} is the voltage amplitude and ω_{inj} is the angular frequency of the injected signal. The output of the oscillator can be expressed as

$$v(t) = V(t)\exp\{j[\omega_{inj}t + \phi(t)]\}, \quad (\text{A2})$$

where $V(t)$ is the envelope of the oscillator output and $\phi(t)$ is the output phase modulation due to the presence of the injected signal.

By considering the nonlinear voltage-current dependence of the nonlinear element as

$$i_{NL}(t) = -G_a v(t) + G_b [v(t)]^3, \quad (\text{A3})$$

where G_a and G_b are constants depending on the current-voltage characteristic curve of the nonlinear device, the circuit of Fig. 11 can be described by [62]

$$\frac{da}{dt'} = \eta(1 - a^2)a + \kappa' \cos \phi, \quad (\text{A4})$$

$$\frac{d\phi}{dt'} = -\Omega' - \frac{\kappa'}{a} \sin \phi, \quad (\text{A5})$$

where a and ϕ are the normalized amplitude and phase of oscillation, respectively. Here, Eqs. (A4) and (A5) are written in a dimensionless form. The time is redefined as $t' = t\omega_0/Q$, where t is the physical time, $\omega_0 = \sqrt{1/LC}$ is the free-running frequency of the oscillator, and $Q = \omega_0 C/G$ is the quality factor of the oscillator. The variables and parameters of

Eqs. (A4) and (A5) are related to the physical quantities as follows. $a(t') = V(t')/V_{OS}$, $\eta = (G_a - G)/2G$, $\kappa' = V_{inj}/2V_{OS}$, $\Omega' = (\omega_{inj} - \omega_0)Q/\omega_0$, $V_{OS}^2 = 4(G_a - G)/3G_b$. Note that, in contrast to Ref. [62], a minus sign appears in the detuning term in Eq. (A5). This is because we write the phase modulation with the plus sign in Eq. (A2), in order to keep consistency with the usual choice in laser analysis, which we also perform in this work.

Variations of the parameter η do not change the qualitative dynamical scenario of the nonlinear oscillator model given by Eqs. (A4) and (A5), since it acts just as a scale factor and can be eliminated from the model equations by the rescaling $\Omega = \Omega'/\eta$, $\kappa = \kappa'/\eta$, and $\tau = t'\eta$. Performing this additional step, we obtain

$$\frac{da}{d\tau} = (1 - a^2)a + \kappa \cos \phi, \quad (\text{A6})$$

$$\frac{d\phi}{d\tau} = -\Omega - \frac{\kappa}{a} \sin \phi, \quad (\text{A7})$$

which have the same form of Eqs. (2) and (3).

APPENDIX B: CUBIC LASER MODEL WITH EXTERNAL OPTICAL INJECTION

Certain types of lasers can be described by the so-called class-A laser model [63]

$$\frac{dE}{dt} = \left(-1 + \frac{\Gamma}{1 + |E|^2}\right)E, \quad (\text{B1})$$

where E is the complex electric field amplitude and Γ is the pump. We can perform a further simplification in this model by approximating $1/(1 + |E|^2)$ by $1 - |E|^2$, obtaining the cubic laser model, which is usually considered the simplest laser model [63]

$$\frac{dE}{dt} = [-1 + \Gamma(1 - |E|^2)]E. \quad (\text{B2})$$

By defining the new pump parameter $P = \Gamma - 1$ and rescaling the electric field to $\tilde{E} = \sqrt{\frac{\Gamma}{\Gamma-1}}E$, Eq. (B2) can be rewritten as

$$\frac{d\tilde{E}}{dt} = P(1 - |\tilde{E}|^2)\tilde{E}. \quad (\text{B3})$$

By considering an external monochromatic optical injection, a term taking into account the injected light must be added in Eqs. (B1), (B2), or (B3). Thus, in the cubic laser model, given by Eq. (B3), we add the term $\tilde{E}_{inj} = \tilde{K}' \exp(j\Delta t)$, where $\Delta \equiv \omega_{inj} - \omega_0$ is the frequency detuning between the external light source and the solitary laser [64]. In this case, in terms of amplitude and phase of the electric field $\tilde{E} = \tilde{R} \exp(j\psi)$, where $\psi = \Delta t + \phi$, the cubic laser model subject to optical injection reads

$$\frac{d\tilde{R}}{dt} = P(1 - \tilde{R}^2)\tilde{R} + \tilde{K}' \cos \phi, \quad (\text{B4})$$

$$\frac{d\phi}{dt} = -\Delta' - \frac{\tilde{K}'}{\tilde{R}} \sin \phi. \quad (\text{B5})$$

The above equations are mathematically the same as those of the electronic circuit model with injected signal [Eqs. (A4) and (A5)]. Here, the pump parameter P plays the role of the parameter η in the circuit model; it can be eliminated from the

laser model by rescaling the time and injection parameters. By defining $\tau = tP$, $\Delta = \Delta'/P$, and $\tilde{K} = \tilde{K}'/P$, the equations of the optically injected laser model read

$$\frac{d\tilde{R}}{d\tau} = (1 - \tilde{R}^2)\tilde{R} + \tilde{K} \cos \phi, \quad (\text{B6})$$

$$\frac{d\phi}{d\tau} = -\Delta - \frac{\tilde{K}}{\tilde{R}} \sin \phi, \quad (\text{B7})$$

which have the same form of Eqs. (2) and (3).

-
- [1] A. T. Winfree, *The Geometry of Biological Time* (Springer-Verlag, New York, 1980).
- [2] Y. Kuramoto, *Chemical Oscillations, Waves, and Turbulence* (Springer-Verlag, Berlin, 1984).
- [3] A. Pikovsky, M. Rosenblum, and J. Kurths, *Synchronization: A Universal Concept in Nonlinear Science* (Cambridge University Press, New York, 2001).
- [4] S. H. Strogatz, *Sync: The Emerging Science of Spontaneous Order* (Hyperion, New York, 2003).
- [5] A. G. Balanov, N. B. Janson, D. E. Postnov, and O. V. Sosnovtseva, *Synchronization: From Simple to Complex* (Springer, Berlin, 2009).
- [6] N. Minorsky, *Nonlinear Oscillation* (Van Nostrand, Princeton, NJ, 1962).
- [7] C. Hayashi, *Nonlinear Oscillations in Physical Systems* (McGraw-Hill, New York, 1964).
- [8] J. Guckenheimer and P. Holmes, *Nonlinear Oscillations, Dynamical Systems and Bifurcation of Vector Fields* (Springer-Verlag, New York, 1983).
- [9] J. M. T. Thompson and H. B. Stewart, *Nonlinear Dynamics and Chaos* (Wiley, Chichester, 2002).
- [10] D. Z. Goodson, in *Mathematical Physics in Theoretical Chemistry*, edited by S. M. Blinder and J. E. House (Elsevier, Amsterdam, 2019).
- [11] G. J. Gbur, *Singular Optics* (CRC Press, Boca Raton, FL, 2017).
- [12] J. M. Greene, *J. Geophys. Res.* **93**, 8583 (1988).
- [13] J. Eggers and M. A. Fontelos, *Singularities: Formation, Structure, and Propagation* (Cambridge University Press, Cambridge, 2015).
- [14] E. M. Izhikevich, *Dynamical Systems in Neuroscience: The Geometry of Excitability and Bursting* (MIT, Cambridge, MA, 2007).
- [15] B. Lindner, J. García-Ojalvo, A. Neiman, and L. Schimansky-Geier, *Phys. Rep.* **392**, 321 (2004).
- [16] P. R. Prucnal, B. J. Shastri, T. F. de Lima, M. A. Nahmias, and A. N. Tait, *Adv. Opt. Photon.* **8**, 228 (2016).
- [17] A. A. Andronov, A. A. Vitt, and S. E. Khaikin, *Theory of Oscillators* (Pergamon Press, Oxford, 1966).
- [18] M. L. Cartwright, *J. Inst. Elec. Eng.* **95**, 88 (1948).
- [19] D. G. Aronson, G. B. Ermentrout, and N. Koppel, *Physica D* **41**, 403 (1990).
- [20] S. Wieczorek, B. Krauskopf, and D. Lenstra, *Opt. Commun.* **172**, 279 (1999).
- [21] M. Frichembruder, R. Pakter, G. Gerhardt, and F. B. Rizzato, *Phys. Rev. E* **62**, 7861 (2000).
- [22] J. Thévenin, M. Romanelli, M. Vallet, M. Brunel, and T. Erneux, *Phys. Rev. Lett.* **107**, 104101 (2011).
- [23] L. K. Li and M. P. Juniper, *J. Fluid Mech.* **735**, R5 (2013).
- [24] B. Kelleher, D. Goulding, B. Baselga Pascual, S. P. Hegarty, and G. Huyet, *Phys. Rev. E* **85**, 046212 (2012).
- [25] J. Pausch, C. Otto, E. Tylaite, N. Majer, E. Schöll, and K. Lüdge, *New J. Phys.* **14**, 053018 (2012).
- [26] M. Romanelli, L. Wang, M. Brunel, and M. Vallet, *Opt. Express* **22**, 7364 (2014).
- [27] C. J. Lin, M. AlMulla, and J. M. Liu, *IEEE J. Quantum Elect.* **50**, 1 (2014).
- [28] A. Thorette, M. Romanelli, M. Brunel, and M. Vallet, *Opt. Lett.* **41**, 2839 (2016).
- [29] M. Romanelli, A. Thorette, M. Brunel, T. Erneux, and M. Vallet, *Phys. Rev. A* **94**, 043820 (2016).
- [30] P. Couillet, D. Daboussy, and J. R. Tredicce, *Phys. Rev. E* **58**, 5347 (1998).
- [31] S. Wieczorek, B. Krauskopf, and D. Lenstra, *Phys. Rev. Lett.* **88**, 063901 (2002).
- [32] D. Goulding, S. P. Hegarty, O. Rasskazov, S. Melnik, M. Hartnett, G. Greene, J. G. McInerney, D. Rachinskii, and G. Huyet, *Phys. Rev. Lett.* **98**, 153903 (2007).
- [33] B. Kelleher, D. Goulding, S. P. Hegarty, G. Huyet, Ding-Yi Cong, A. Martinez, A. Lematre, A. Ramdane, M. Fischer, F. Gerschütz, and J. Koeth, *Opt. Lett.* **34**, 440 (2009).
- [34] B. Kelleher, C. Bonatto, P. Skoda, S. P. Hegarty, and G. Huyet, *Phys. Rev. E* **81**, 036204 (2010).
- [35] B. Kelleher, C. Bonatto, G. Huyet, and S. P. Hegarty, *Phys. Rev. E* **83**, 026207 (2011).
- [36] M. Turconi, B. Garbin, M. Feyereisen, M. Giudici, and S. Barland, *Phys. Rev. E* **88**, 022923 (2013).
- [37] B. Romeira, J. Javaloyes, C. N. Ironside, J. M. L. Figueiredo, S. Balle, and O. Piro, *Opt. Express* **21**, 20931 (2013).
- [38] A. Hurtado and J. Javaloyes, *App. Phys. Lett.* **107**, 241103 (2015).
- [39] B. Romeira, R. Avó, J. M. L. Figueiredo, S. Barland, and J. Javaloyes, *Sci. Rep.* **6**, 19510 (2016).
- [40] B. Garbin, A. Dolcemascolo, F. Prati, J. Javaloyes, G. Tissoni, and S. Barland, *Phys. Rev. E* **95**, 012214 (2017).
- [41] J. Robertson, T. Deng, J. Javaloyes, and A. Hurtado, *Opt. Lett.* **42**, 1560 (2017).
- [42] A. Dolcemascolo, B. Garbin, B. Peyce, R. Veltz, and S. Barland, *Phys. Rev. E* **98**, 062211 (2018).
- [43] M. Dillane, B. Tykalewicz, D. Goulding, B. Garbin, S. Barland, and B. Kelleher, *Opt. Lett.* **44**, 347 (2019).
- [44] J. Robertson, E. Wade, and A. Hurtado, *IEEE J. Sel. Topics Quant. Electron.* **25**, 5100307 (2019).
- [45] M. Dillane, I. Dubinkin, N. Fedorov, T. Erneux, D. Goulding, B. Kelleher, and E. A. Viktorov, *Phys. Rev. E* **100**, 012202 (2019).
- [46] H. L. Hodgkin, *J. Physiol.* **107**, 165 (1948).
- [47] J. Rinzel and G. B. Ermentrout, in *Methods in Neuronal Modeling*, edited by C. Koch and I. Segev (MIT, Cambridge, MA, 1989).
- [48] E. M. Izhikevich, *Int. J. Bifurcat. Chaos* **10**, 1171 (2000).

- [49] S. A. Prescott, Y. De Koninck, and T. J. Sejnowski, *PLoS Comput. Biol.* **4**, e1000198 (2008).
- [50] S. Wicczorek, P. Ashwin, C. M. Luke, and P. M. Cox, *Proc. R. Soc. A* **467**, 1243 (2011).
- [51] P. De Maesschalck and M. Wechselberger, *J. Math. Neurosci.* **5**, 16 (2015).
- [52] In semiconductor lasers, the locking region is asymmetric, due to the linewidth enhancement factor, and the saddle-node bifurcation can extend to large injection strength values at one side of the frequency detuning [31,35].
- [53] R. Adler, *Proc. IRE* **34**, 351 (1946).
- [54] A. W. Gillies, *Quart. J. Mech. Appl. Math.* **7**, 152 (1954).
- [55] P. J. Holmes and D. A. Rand, *Q. Appl. Math.* **35**, 495 (1978).
- [56] W. L. Kath, *Stud. Appl. Math.* **65**, 95 (1981).
- [57] N. S. Namachchivaya and S. T. Ariaratnam, *SIAM J. A. Math.* **47**, 15 (1987).
- [58] Y. Zhang and M. Golubitsky, *SIAM J. Appl. Dynam. Sys.* **10**, 1272 (2011).
- [59] L. M. Childs and S. H. Strogatz, *Chaos* **18**, 043128 (2008).
- [60] E. J. Doedel, A. R. Champneys, T. Fairgrieve, Yu. Kuznetsov, B. Oldeman, R. Pfaffenroth, B. Sandstede, X. Wang, and C. Zhang, AUTO-07P, Continuation and bifurcation software for ordinary differential equations, Technical report, Concordia University Montreal (2007).
- [61] L. I. Manevitch, A. S. Kovaleva, V. V. Smirnov, and Yu. Starosvetsky, *Nonstationary Resonant Dynamics of Oscillatory Chains and Nanostructures* (Springer Nature, Singapore, 2018).
- [62] I. Ali, A. Banerjee, A. Mukherjee, and B. N. Biswas, *IEEE Trans. Circ. Syst. I* **59**, 137 (2012).
- [63] L. Lugiato, F. Pratti, and M. Brambilla, *Nonlinear Optical Systems* (Cambridge University Press, Cambridge, 2015).
- [64] T. Erneux and P. Glorieux, *Laser Dynamics* (Cambridge University Press, Cambridge, 2010).